ScientificScholar®
Knowledge is power
Publisher of Scientific Journals

https://arabjchem.org

Arabian Journal of Chemistry

Article in Press

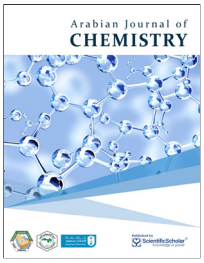

Original Article

# Fabrication of mesoporous beta zeolites for lead ion adsorption from aqueous solutions

Xuefeng Li*, Shanshan Li

*College of Chemistry and Materials Engineering, Xuchang University, Xuchang, Henan, China*

ARTICLE INFO

*Keywords:*
Acid base treatment
Lead ion adsorption
Mesoporous Beta zeolite

ABSTRACT

Mesoporous beta zeolites were fabricated by treating the parent beta zeolite (B) with two base-acid (BAB) and acid-base (ABB) treatment methods. These zeolites were characterized by X-ray diffraction, $N_2$-adsorption, and lead ion adsorption performance in aqueous solution. BAB and ABB retain the main beta phase characteristics and display mesoporous characteristics, while ABB exhibits a drastic decrease in crystallinity and a substantial increase in nitrogen adsorption compared with BAB. The ABB adsorption ratio and quantity for lead ion reach 90.3% and 23.95 mg/g, which are higher than those of B and BAB under better conditions. Additionally, the results for ABB effectively fit the pseudo-second-order adsorption equation and the Freundlich adsorption model that predicts their lead ion adsorption being multilayer coverage one. Therefore, as a novel mesoporous zeolite, ABB is an excellent lead ion adsorbent and has the potential to remove other metal ions and even organic adsorbates. Also, method 2 (acid-base treatment) is a more effective approach for the synthesis of mesoporous zeolites and even other advanced materials.

## 1. Introduction

Over the past decades, industrial development and continual urbanization have led to growing waste production problems. They include pesticides, pigments and dyes, heavy metals, and drug removal treatments. Among these waste products, heavy metals are the most dangerous [1] because their release into water bodies in certain amounts (such as lead, copper, nickel, chromium, and cadmium) can cause high toxicity to the human body, including carcinogenicity, teratogenicity, and mutagenicity. Moreover, they can accumulate in living organisms without being biodegraded, resulting in various disorders and diseases even at low concentrations [2]. For instance, as a toxic contaminant, lead is frequently found in industrial and productive wastewater during the manufacturing process of storage batteries, leaded glasses, pigments, paints, and dyeing and printing materials [3]. Lead exposure can cause many health risks for humans, including damage to the liver, kidney, and brain to induce mental retardation. Since lead pollution in soil and water bodies can cause many hazardous impacts on human beings, effective ways need to be developed to prevent this pollution [3] or to recycle the waste lead for further industrial utilization. Therefore, recycling heavy metals for the benefit of environmental or resource reutilization has become a significant research topic.

Many approaches have been implemented to remove heavy metals from water or aqueous mixtures; these include complexation, reverse osmosis, ion exchange, physical adsorption, precipitation neutralization, and sequestration [4]. Among them, the adsorption method is widely preferable owing to its advantages of easy operation, high efficiency, cost-effectiveness, and easy attainment of various widely used adsorbents, such as carbon materials, inorganic oxides, clay, polymeric materials, agricultural byproducts, and metal organic framework (MOFs) [3-9]. As a kind of special inorganic oxide, zeolite has been prioritized for application in research and industrial areas due to its orderly pore structure, high specific area, and ion exchangeability. Several previous studies have indicated that heavy metal ions can be removed or adsorbed by various zeolites, including Beta [10], Y [11], and ZSM-5 [12].

In addition to their use as adsorbents, zeolites can also be utilized as catalysts. However, the pore diameters of zeolites are less than 1 nm, limiting the access of bulky substrates to active sites on their surface. For this reason, a novel kind of zeolite, termed hierarchical zeolite or mesoporous zeolite, has been developed with better performance than the parent zeolite in catalyzing various reactions [13-14]. Accordingly, this novel hierarchical or mesoporous zeolite has the potential for use as an adsorbent for organic pollutants largely due to its mesoporous pore structure. For instance, mesoporous modified-HMOR and HZSM-5 samples were prepared by alkaline and/or acid treatment, including soaking, leaching, and ion exchange of microporous parent zeolites, and the obtained mesoporous zeolites exhibited a higher adsorption rate and capacity than microporous zeolites for the removal of sulfuron methyl [15]. What's more, many papers reported various mesoporous zeolites as adsorbents for the removal of organic dyes, drugs, petroleum products, and volatile waste [16-18]. However, to date, only a few studies have been performed on removing metal ions with hierarchical or mesoporous zeolites, such as modified clinoptilolite, Y zeolite, and Chabazite (CHA)-type zeolite[19-21]. To our knowledge, a study on the mesoporous beta zeolite for the adsorption of heavy metals has not been published in the past decades.

Therefore, we conducted the present research work to search for a better method for fabricating the mesoporous beta zeolite and further verify if this novel material possesses a preferable performance on the adsorption of lead ions. Specifically, in this context, we prepared the mesoporous beta zeolites with two methods: sequential base-

*Corresponding author:
*E-mail address:* snow_mount@163.com (X. Li)

**Received:** 24 November, 2024 **Accepted:** 19 February, 2025 **Epub Ahead of Print:** 24 April 2025 **Published:** ***
**DOI:** 10.25259/AJC_190_2024

acid treatment and sequential acid-base treatment. We also explored the lead ion removal performance in water between the parent Beta zeolite and the two mesoporous zeolites by their use as adsorbents. Additionally, the characteristics of the adsorbents and the optimized adsorption conditions were also systematically investigated.

## 2. Materials and Methods

### 2.1. Materials

In this study, all the chemicals used were of AR grade: beta zeolite (≧ 99.0%, Shanghai Research Institute of PetroChemical Technology, Shanghai, China), sodium hydroxide (NaOH), and tetrabutylammonium bromide (TBAB) (≧ 99.0%, Guoyao Chemical Reagent Co., Ltd., Jiangsu, China), lead nitrate (≧ 99.99%, Tianjin Yaohua Chemical Reagent Co., Ltd., Tianjin, China), citric acid (≧ 99.5%, Tianjin Fuchen Chemical Reagent Factory, Tianjin, China), ammonium fluoride (≧ 99.0%, Xilong Science Co., Ltd. Guangdong, China), and ammonium nitrate (≧ 99.0%, Beijing Hongxing Chemical Plant, Beijing, China). Deionized water was obtained from Xuchang University (0.1-1 MΩ·cm, Henan, China).

### 2.2. Preparation of mesoporous Beta zeolite using method 1

Beta zeolite powder (20 g, B), TBAB (9.3 g), and NaOH (300 mL, 0.2 mol/L) were mixed in a 500 mL four-necked flask, followed by magnetic agitation at 80°C for 30 mins. After centrifugation, the solid product was obtained, dried at 90°C, and calcined at 550°C; the final product was denoted as base-beta (BB). Next, three consecutive ammonium exchanges were carried out to recover a $H^+$ form zeolite. Subsequently, the $H^+$ form BB was treated with citric acid (300 mL, 0.06 mol/L) at 60°C for 1 h under stirring, followed by centrifugation, washing, drying, and calcination. The final product was denoted as BAB, with A representing the acid (citric acid) treatment and BAB representing the base and sequential acid treatment of Beta zeolite [22].

### 2.3. Preparation of mesoporous Beta zeolite using method 2

Briefly, 20 g of Beta zeolite (B) was ground into powder and mixed with $NH_4F$ solution (100 mL, 0.36 mol/L), followed by agitation at room temperature (RT), dried, and then subjected to calcination to obtain sample AB, with sample A for acid ($NH_4F$) treatment. Next, sample AB (3 g) was subjected to base treatment (90 mL 0.2 mol/L NaOH solution) at 80°C for 60 mins. After centrifugation, the base-treated sample was obtained, followed by washing and drying. After conversion to $H^+$, the final product was defined as ABB, with B representing the base (NaOH) treatment [23].

Methods 1 and 2 have been illustrated in Scheme 1.

### 2.4. Characterization of the B, BAB and ABB zeolite samples

X-ray diffraction (XRD) characterization of the three samples was performed on a PHILIPS X'Pert-MPD PW3050 diffractometer (Tokyo, Japan) under the conditions: Cu$K_\alpha$ radiation, 40 kV tube voltage, λ=0.15418 nm, 30 mA tube current, 10°-90° angle range and 2°/min scanning speed.

After degassing and treating all samples at 200°C for 3 hrs, $N_2$-adsorption-desorption characterization analysis was conducted at –196 °C on a Micrometrics ASAP 2010 automated instrument. The specific surface area and pore size of the three samples were investigated by Brunauer-Emmett-Teller (BET) and Barret-Joyner-Halenda (BJH) analysis, respectively.

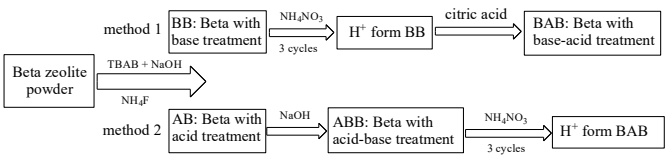


**Scheme 1.** Flow diagram of synthesis methods of (1) BAB and (2) ABB.

### 2.5. Lead ion adsorption experiments

Briefly, 25 mL of lead nitrate solution (100 mg/L) and a given mass of zeolite sample were poured into a capped conical flask (50 mL), followed by oscillation of the flask for a certain amount of time to ensure thorough adsorption and removal of lead ions. Next, the mixture was collected and filtered to obtain 100 mL of supernatant in a volumetric flask, and the residual lead ion concentration in the adsorbed solution was measured through spectrophotometry on an atomic adsorption spectrophotometer (WFX-1F2B2, China). The lead ion adsorption quantity ($Q$, mg/g) and adsorption and adsorption ratio ($R$, %) were determined using Eqs (1) and (2), respectively.

$$Q = 1/C_b \times (C_0 - C_e) \quad (1)$$

$$R = 1/C_0 \times (C_0 - C_e) \times 100\% \quad (2)$$

where $C_0$ represents the initial lead ion concentration (mg/L), $C_e$ is the equilibrium lead ion concentration (mg/L), and $C_b$, is the zeolite amount of each sample (g/L).

The adsorption conditions and principles were investigated through three groups of batch adsorption experiments, with the zeolite amount, initial lead ion concentration, and treatment time selected as variables, while the treatment temperature (RT) and pH (initial pH) were considered constants. The detailed conditions for each adsorption experiment have been described in the following section.

## 3. Results and Discussion

### 3.1. Characterization results of the B, BAB, and ABB zeolite samples

Figure 1 displays the XRD characterization results of the parent beta zeolite (B) and its modified analogs (BAB and ABB). B displays a typical diffraction pattern of the Beta zeolite, including a very strong and sharp peak at 2$\theta$ = 22.5° and several weak peaks at 2$\theta$ = 11.8, 13.4, 14.5, 21.4, 25.4, 27, 28.8, 29.8, 43.5, and 56°. Moreover, the two modified samples exhibit a remarkable crystallinity reduction. For instance, ABB shows the absence of nearly all peaks except for a strong intense peak at 2$\theta$ = 22.5°, while at 2$\theta$ = 22.5°, BAB also displays a strong, intense peak, but with various weak peaks at 2$\theta$ = 13.4°, 14.5°, 21.4°, 25.4°, 27°, and 43.5°, ascribed to the retention of beta zeolite characteristics. These observations indicate that the microcrystalline structures of the two samples were damaged by the acid and base treatments; a larger damage extent was observed for ABB than for BAB. However, the main structural characteristics (2$\theta$ = 22.5°) of the beta zeolite are maintained for these two samples, despite the absence of the other crystalline diffraction patterns of the beta zeolite. Accordingly, both BAB and ABB could be considered beta-type zeolites. To probe their structural properties, the three samples were further investigated in subsequent characterization tests [23-26]. Figures 2, 3, and Table 1 show the $N_2$ adsorption-desorption characterization results, the BJH analysis results (pore structure), and the physical characteristic data of the three samples, respectively. According to the IUPAC standard, the parent zeolite beta (B) exhibits an I-type isotherm accompanied

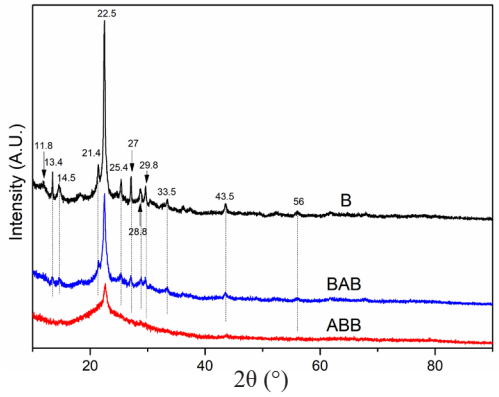


**Figure 1.** XRD analysis results indicating a serious crystallinity decrease for ABB while a good crystallinity retaining for BAB. The black line represents the sample B (Beta zeolite).

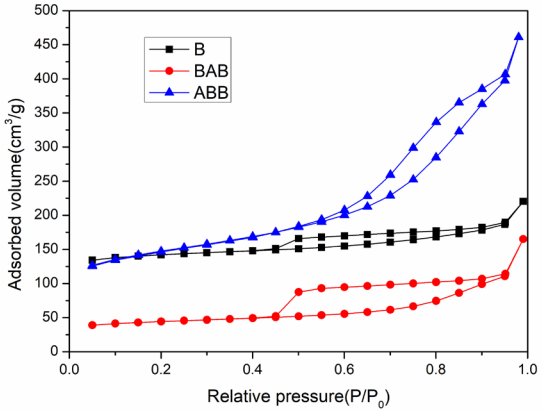


**Figure 2.** Nitrogen adsorption-desorption analysis results indicating a large nitrogen-adsorption volume increase for ABB while a substantial volume decrease for BAB.

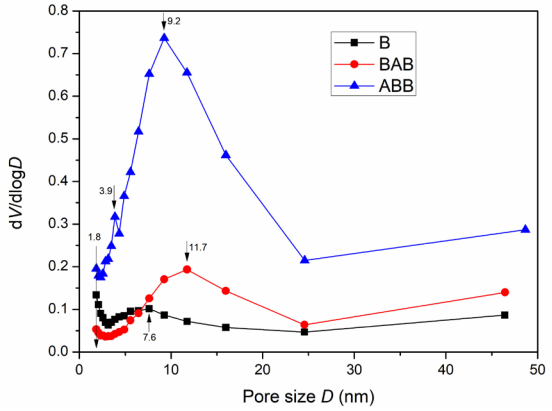


**Figure 3.** Pore structure analysis results indicating mesoporous characteristics for both ABB and BAB with mesoporous pores.

**Table 1.** Physical structure characterization results from the three samples.

| Sample | $A_{BET}$(m²/g)[a] | $D_{aapd}$(nm)[b] | $D_{mpd}$(nm)[c] | $V_{tpv}$(cm³/g)[d] |
|---|---|---|---|---|
| B | 459.08 | 7.1918 | ≦1.8; 7.6 | 0.341 |
| BAB | 147.58 | 11.9864 | 11.7 | 0.256 |
| ABB | 496.12 | 8.064 | 9.2 | 0.713 |

Notes: [a]BET specific surface area; [b]BJH adsorption average pore diameter (4*V*/*A*); [c]Most probable distribution pore size; [d]Total pore volume.

by an H4-type hysteresis loop [27], indicating that zeolite beta is a combination of a microporous and limited mesoporous material. This deduction can also be confirmed by the observation that the beta zeolite possesses not only micropores but also mesopores (11.7 nm), as shown in Figure 3. After treatment with base followed by acid, BAB has a similar isotherm to that of beta zeolite with a wider and larger hysteresis loop. Furthermore, the pore volume of BAB is lower than that of B (0.256 $cm^3/g$ versus 0.341 $cm^3/g$). Evidently, these changes enabled BAB to develop the most probable distribution pore size of 11.7 nm, which is characteristic of a mesoporous material. Moreover, ABB exhibits an IV-type isotherm, coupled with a H3-type hysteresis loop, which is the key feature of a highly mesoporous material. More importantly, the most probable distribution pore size of ABB is 9.2 nm, with a pore volume of 0.713 $cm^3/g$, which is significantly larger than that of both B (0.341$cm^3/g$) and BAB (0.256 $cm^3/g$) [25-26, 28]. Moreover, the three samples have different specific surface areas, with sizes in the order of ABB > B > BAB based on their respective adsorption volumes; these results indicate that the impact of acid-base treatment is more pronounced than that of base-acid treatment.

From the above-mentioned XRD and $N_2$-adsorption results, it is demonstrated that both two mesoporous zeolites are successfully

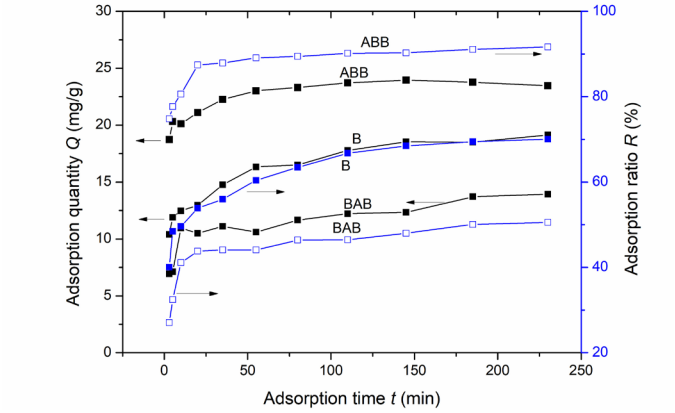


**Figure 4.** Impacts of adsorption time on the quantity of lead ions adsorbed on the three samples. Results: ABB having a higher adsorption quantity and an adsorption ratio than B or BAB.

fabricated by base-acid treatment and acid-base treatment, respectively. ABB acquires a large nitrogen adsorption volume increase despite a serious crystallinity decrease. On the contrary, BAB suffers from a substantial nitrogen adsorption volume decrease despite retaining a good crystallinity. As a result, compared with method 1 (base-acid), method 2 (acid-base) can be preferred for obtaining "real" mesoporous zeolites.

### *3.2 Adsorption of the lead ions*

#### *3.2.1. Relationship between the lead ion adsorption performance and adsorption time*

Figure 4 displays the dependence of the lead ion adsorption performance on the adsorption time (3 to 230 mins) for B, BAB and ABB, and the other parameters were as follows: 4 g/L adsorbent dosage, RT adsorption, and 114 mg/L lead ion concentration. Clearly, for each sample, both the adsorption ratio and adsorption quantity rapidly increase at the initial stage, followed by a slow increase before finally reaching a saturation state. The three-stage trend follows the adsorption model of a substance in solution to a porous material, and three explanations are possible. First, in the early adsorption stage, adsorption mainly occurs on the adsorbent's outer surface, enabling a significant increase in the adsorption rate. In the second stage, the rate of increase in the adsorption ratio decreases, possibly due to a decrease in the lead-ion concentration in the solution. Another possible explanation is that during the second stage, adsorption mainly proceeds on the inner surface of the pores of the zeolites, thereby reducing the mass transport speed. Finally, the adsorption reaches a saturation state because the adsorption sites have been occupied, and less lead ion residue is present. This is roughly consistent with the heavy metal ion adsorption trend for other porous materials [12, 14, 29].

In Figure 4, ABB also has a greater adsorption quantity and adsorption ratio than B or BAB, and the adsorption rate for the three samples follows this sequence: ABB > B > BAB; these results indicate that ABB has best performance, and that BAB has the worst performance with respect to the lead ion adsorption. For ABB, adsorption saturation occurs within 145 mins, with a maximal adsorption capacity of 23.95 mg/g and a removal ratio of 90.3%.

#### *3.2.2. Relationship between the lead ion adsorption performance and adsorbent dosage*

Figure 5 shows the impact of the adsorbent dosage (1–6 g/L) on the lead ion adsorption performance of the three samples. The adsorption tests were performed at a lead ion concentration of 114 mg/L, an adsorption time of 150 mins and RT. ABB outperforms both B and BAB with respect to the lead ion adsorption under the test conditions. Specifically, the adsorption ratio of ABB rapidly increases and reaches 79.7% as the adsorbent dosage increases from 1 to 2.5 g/L; this was followed by a slow increase of up to 92.3% at the 5 g/L dosage.

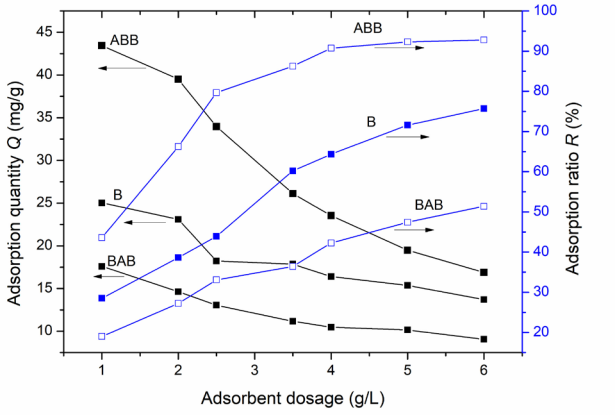


**Figure 5.** Impacts of the different adsorbent amounts on the quantity of lead ion adsorbed on the three samples. Results: ABB having a higher adsorption quantity and an adsorption ratio than both B and BAB.

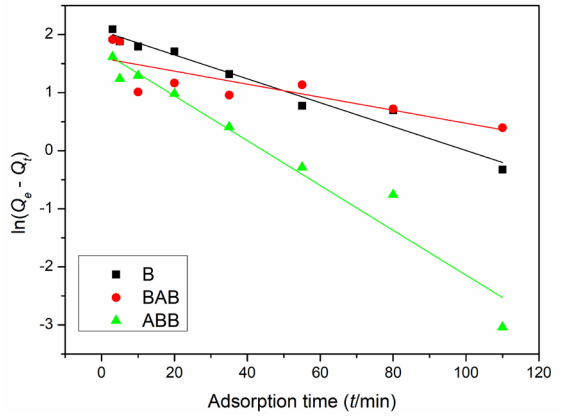


**Figure 7.** Lead ion adsorption quantities on the three samples at different adsorption time points fitted by the pseudo-first-order adsorption equation. Results: well-fitting for BAB and ABB while an obvious deviation for B.

Finally, the adsorption ratio remains almost unchanged at 92.8% as the dosage further increases to 6 g/L. These results indicate that a dosage of 5 g/L adsorbent is sufficient to meet the adsorption requirements in the following tests. After reaching a 92.3% adsorption ratio, the low residual lead-ion concentration in the solution may cause the adsorption rate to reach a plateau at a higher adsorbent dosage [30-32]. However, compared with that of ABB, the adsorption ratios of B and BAB linearly and slowly increase. Additionally, in the total dosage range, ABB has a greater adsorption ratio and adsorption quantity than B or BAB. Therefore, ABB has the optimal performance in terms of lead ion adsorption among the three samples.

### *3.2.3. Relationship between the lead ion adsorption performance and its initial concentration*

The relationships of the lead ion adsorption ratio and adsorption quantity with the initial lead ion concentration in the range of 47.5-148.9 mg/L were examined at a 150 min adsorption time and 5 g/L adsorbent dosage. Figure 6 shows that for each of the three adsorbents, the adsorption ratio decreases, and the adsorption quantity increases with increasing initial lead-ion concentration. This potentially occurs because a rise in the initial lead ion concentration can increase the absolute lead ion amount removed by each of the three adsorbents; thus, the adsorption quantity increases when a defined amount of adsorbent is utilized. However, a higher increase in the initial lead ion concentration than in the lead ion removal was reported to reduce adsorption rate [30].

In addition, when a certain amount of adsorbent is used, the adsorption amount becomes fixed, indicating that a higher initial lead-ion concentration can increase the residual lead amount and reduce the removal efficiency; this leads to an increase in the adsorption ratio and a decrease in the adsorption quantity. These reasons are further elucidated in the following sections. Figure 5 shows that ABB has a greater adsorption ratio and a greater adsorption quantity than B and BAB; these results further confirm that ABB has the best lead ion adsorption performance among the three adsorbents.

### *3.2.4. Adsorption kinetic results*

Adsorption kinetics can directly reflect the reaction rate of a process and provide rich information on the adsorption mechanisms; thus, research on adsorption kinetics plays a crucial role in the development of advanced adsorbents [4, 33]. Currently the pseudo-first- and pseudo-second-order equations are commonly utilized to study potential adsorption mechanisms; the former is on the assumption of adsorption rate dependence on adsorption quantity, and the latter involves the chemical adsorption (i.e., electron pair sharing between the adsorbed substance and adsorbent) [34]. In the adsorption kinetic analysis, the adsorption time is used as a function of the adsorption rate (Figure 7). The two models (Eq. (3) for the pseudo-first-order model and Eq. (4) for the pseudo-second-order model) are applied to analyze the lead ion test results [34]:

$$\ln(Q_e - Q_t) = \ln Q_e - k_1 t \quad (3)$$

$$t/Q_t = (Q_e)^2/k_2 + t/Q_e \quad (4)$$

where $k_1$ represents the constant rate of the first-order Eq. (3) (1/min); $k_2$ is the constant rate of the second-order Eq. (4) [g/(mg × min)]; and $Q_e$ and $Q_t$ are the adsorbate amounts (mg/g) at equilibrium (e) and time $t$ (min), and can be obtained by Eq. (1).

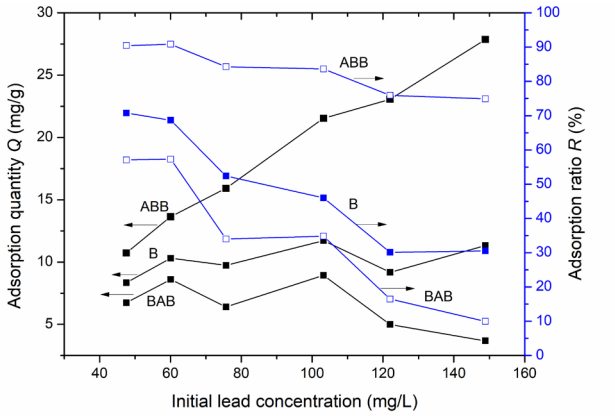


**Figure 6.** Impacts of different initial lead-ion concentrations on the quantity of lead adsorbed on the three samples. Results: ABB having a higher adsorption quantity and an adsorption ratio than B and BAB.

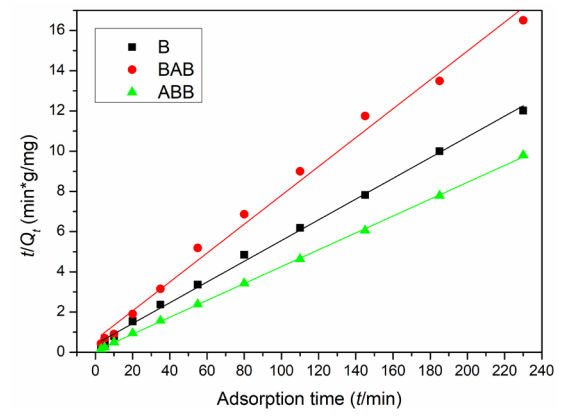


**Figure 8.** Lead ion adsorption quantities on the three samples at different adsorption time points fitted by the pseudo-second-order adsorption equation. Results: better fitting for B, BAB and ABB.

**Table 2.** Adsorption parameters and correlation coefficients for the three samples based on the pseudo-first-and pseudo-second-order adsorption equations.

| | Pseudo-first-order kinetic model | | | | Pseudo-second-order kinetic model | | |
|---|---|---|---|---|---|---|---|
| | $k_1$ (1/min)[b] | $Q_{exp}$ (mg/g)[a] | $Q_{e,cal}$ (mg/g)[c] | $r^{2d}$ | $k_2$ (g/(mg·min))[e] | $Q_{e,cal}$ (mg/g)[c] | $r^{2d}$ |
| B | 0.021 | 19.13 | 7.86 | 0.9649 | 938.292 | 19.39 | 0.9974 |
| BAB | 0.011 | 13.93 | 4.93 | 0.6414 | 309.660 | 13.93 | 0.9917 |
| ABB | 0.039 | 23.95 | 5.56 | 0.9484 | 9107.998 | 23.83 | 0.9997 |

Notes: [a]Maximum adsorption quantity in experimental data; [b]Rate constant; [c]Equilibrium adsorption quantity; [d]Correlation coefficient; [e]Rate constant.

Figures 7 and 8 show the fitting results of the kinetic experimental data, and Table 2 displays the specific parameters. B, BAB, and ABB have linear correlation coefficients ($r^2$) of 0.9649, 0.6414, and 0.9484, respectively, in the first-order model and 0.9974, 0.9917, and 0.9997, respectively, in the second model; these results indicate that all three samples are better fit by the second-order model. Based on this model, ABB has the best adsorption performance among the three samples, and the adsorption quantities are 19.39, 13.93, and 23.83 mg/g for the three samples; these values are much closer to the actual experimental data (19.13, 13.93, and 23.95 mg/g , respectively) than the first model fitting results (7.86, 4.93, and 5.56 mg/g, respectively). Furthermore, based on the $r^2$ values and contrast between plots, the second adsorption fitting model can also be concluded to be better for all three samples; this model has the best match with the adsorption performance of ABB (Table 2).

### 3.2.5 Adsorption isotherm results

Adsorption isotherms can reveal the intrinsic relationship between the adsorbent and adsorbate and provide information regarding the adsorption quantity of the adsorbent with respect to the adsorbate; thus, these isotherms have been regarded as the most crucial experimental results in adsorption studies [4]. In this study, we used two common and prevalent isotherms (Langmuir and Freundlich) to further explore the relationship between the equilibrium concentration ($C_e$) and adsorption quantity ($Q_e$) of the three adsorbents for lead ion adsorption [31]. The two isotherms can be transformed into linear forms and expressed by Eqs. (5) and (6) [4].

$$C_e/Q_e = 1/(bQ_{max}) + C_e/(Q_{max}) \text{ (Langmuir isotherm)} \quad (5)$$

where $C_e$ indicates the adsorbate equilibrium concentration (mg/L); $Q_e$ is the adsorbate amount (mg/g) at equilibrium (e); $Q_{max}$ is the monolayer maximal adsorption quantity of the adsorbent upon saturation of its surface with the adsorbate molecules and is the maximal adsorption quantity (mg/g); and $b$ (L/mg) is a Langmuir coefficient associated with the adsorption energy. The Langmuir model is established by assuming the formation of a saturated monolayer under the condition of the maximal quantity of the adsorbate on the surface of the adsorbent [4], and both $Q_{max}$ and $b$ can be estimated based on the plot of $C_e/Q_e$ vs $C_e$, respectively.

$$\ln Q_e = \ln K_F + (\ln C_e)/n \text{ (Freundlich isotherm)} \quad (6)$$

where $K_F$ represents the adsorbent's adsorption quantity and $1/n$ is the adsorption strength. $1/n$ and $K_F$ can be obtained based on the linear graphs of $\ln Q_e$ and $\ln C_e$, respectively. The Freundlich adsorption model is established on the assumption of multilayer adsorption, which is a continuous and uneven adsorption of an adsorbate on the surface of an adsorbent even after saturation equilibrium [30].

According to the fitting results in Figures 9 and 10 and Table 3, the $r^2$ values using the Langmuir model are 0.2226, 0.1545, and 0.9226, and the $r^2$ values using Freundlich model are 0.1044, 0.3354, and 0.9392 for B, BAB, and ABB, respectively. These data indicate that the ABB experimental data are effectively fit by the isotherms of both the Langmuir and Freundlich models, while the B and BAB experimental data clearly deviate from the two models. Due to higher $r^2$ value using the Freundlich model than that of Langmuir model, the lead ion

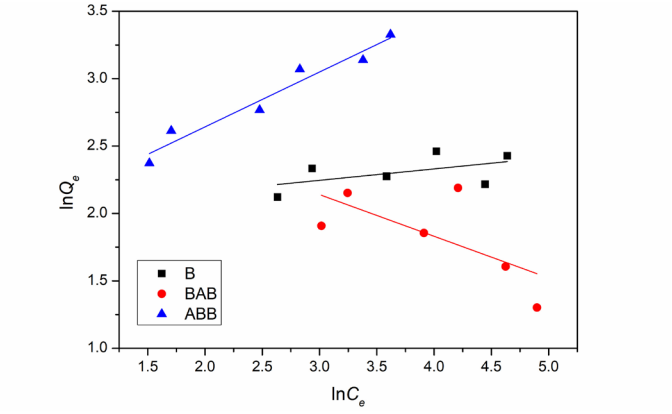


**Figure 9.** Lead ion adsorption quantities and equilibrium concentrations on the three samples fitted by the Langmuir adsorption model. Results: serious deviations for B and BAB while well fit for ABB.

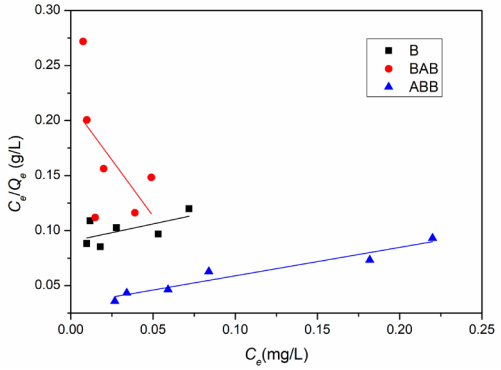


**Figure. 10.** Lead ion adsorption quantities and equilibrium concentrations on the three samples fitted by the Freundlich adsorption model. Results: serious deviations for B and BAB while better fit for ABB.

**Table 3.** Adsorption parameters and correlation coefficients for the three samples based on both Langmuir and Freundlich adsorption models.

| | Langmuir model | | | Freundlich model | | |
|---|---|---|---|---|---|---|
| | $Q_{max}$(mg/g)[a] | $b$ (L/mg)[b] | $r^{2c}$ | $K_F$[d] | $n$[e] | $r^{2c}$ |
| B | 3.15 | 3.519 | 0.2226 | 7.335 | 11.840 | 0.1044 |
| BAB | –0.49 | –9.464 | 0.1545 | 21.483 | –3.235 | 0.3354 |
| ABB | 3.87 | 7.803 | 0.9226 | 6.220 | 2.455 | 0.9392 |

Notes: [a]Maximum adsorption quantity; [b]Langmuir constant associated with adsorption energy; [c]Correlation coefficient; [d]Capacity of each adsorbent to adsorb lead ions; [e]Reciprocal of adsorption intensity.

adsorption on ABB zeolite can be considered multilayer coverage [30]. It is because that many defect sites, vacancies, or cluster regions in ABB owing to an acid-base damage causes the surface non-uniformity of adsorption sites [12]. Meanwhile, it may be because the hydrated lead ion in initial solution has larger volume than lead ion and therefore cannot be considered as a mass point. These two non-ideal factors result in the compliance of ABB adsorption with the Freundlich rather than the Langmuir model. Future studies will further examine the adsorption trends for B and BAB.

Based on the characterization and adsorption results, the phase of ABB can be concluded to retain its mesoporous characteristics although its structure is greatly damaged. More importantly, among the three samples, ABB exhibits the greatest lead ion adsorption ability since it had the largest pore size. This phenomenon can be qualitatively explained, and the adsorption mechanisms are proposed by two aspects as follows. On the one hand, wider mesoporous pores and more vacancies in ABB compared to those in B and BAB, are beneficial for Pb(II) ions diffusing and interacting with adsorption sites. On the other hand, ABB has more

**Table 4.** Comparison of the adsorption property (maximum adsorption capacity, $Q_{max}$ ($mg \cdot g^{-1}$)) between ABB and different adsorbents reported in the literature for lead ion.

| Adsorbent | Synthesis method | Condition (pH; temperature) | $Q_{max}$ ($mg \cdot g^{-1}$) | References |
|---|---|---|---|---|
| Nanometer MCM-41 | RT | pH 4.5; 25°C | 131.71 | [29] |
| Mesoporous Beta zeolite ABB | Acid-base treatment | Initial pH; RT | 23.95 | Current study |
| $Ca^{2+}$-modified zeolite | Hydrothermal | pH 11.8; RT | 23.36 | [35] |
| Kaolin | Alkaline fusion | pH 6.5; RT | 14.64 | [36] |
| Kazakhstani natural zeolite | — | pH 6.1 RT | 14 | [37] |
| Cellulose-based bio-adsorbents | Papaya peel powder | pH4; 30°C | 6.45 | [32] |
| zeolite/MWCNT | Zeolite with carbon nanotube PAN | Initial pH; 48°C | 5.9 | [38] |
| Oil palm frond | Agricultural waste | pH 3.0; 20°C | 5.32 | [39] |
| CdZnS/ZnS quantum dots | Aqueous colloidal method | pH6.9; 61.1°C | 3.56 | [40] |
| Mesoporous Y zeolite | alkaline treatment | pH6; 25°C | 3.5 | [20] |

MWCNT: multi-walled carbon nanotube, Initial pH means the pH value for the solution without acid or base adjusting.

Si-O-Al, Si-OH and Al–OH clusters exposed on the pore surface after acid-base treatment, which easily leads to the ion exchange reactions or/and electrostatic interactions between Pb ion and H, Al or O atoms [12]. Furthermore, Table 4 lists various types of commercial, natural, and wastes adsorbents applied for lead removal in wastewater in some previous studies [20, 29, 32, 35-40]. It can be seen that except for MCM-41 mesoporous silica, ABB presents the highest adsorption capacity compared with other analogues. Consequently, method 2 (acid-base treatment) is a more effective approach for synthesizing mesoporous zeolites and even other advanced materials. All these results motivate us to further optimize the preparation procedure and elucidate the mechanism of adsorption process in the following work.

## 4. Conclusions

BAB and ABB retain their Beta zeolite XRD patterns and display mesoporous characteristics with mesoporous isotherms and mesopores of 11.7 and 9.2 nm, respectively; these results show the successful preparation of mesoporous beta zeolites by base-acid treatment and acid-base treatment, respectively. However, ABB exhibits a drastic decrease in crystallinity and a substantial increase in nitrogen adsorption volume, while BAB retains good crystallinity and has a substantial decrease in nitrogen adsorption volume. The lead ion adsorption quantities of the three samples follow the sequence of ABB > B > BAB; this result agrees with the order of their adsorption volumes. At 4 g/L adsorbent, 145 min adsorption time, and 114 mg/L lead ion concentration, ABB reaches a lead ion adsorption ratio and adsorption quantity of 90.3% and 23.95 mg/g, respectively. Additionally, the results for ABB are largely fitted by the Freundlich adsorption model, in contrast to the major deviation of B and BAB from both the Langmuir and Freundlich adsorption models. Moreover, the pseudo-second-order adsorption equation effectively fits the experimental results of the three samples; additionally, this equation shows the best match with the performance of ABB and predicts its lead ion adsorption as multilayer coverage adsorption. Therefore, ABB is an excellent lead ion adsorbent and has the potential use for removing other metal ions and even organic adsorbates. Also, method 2 (acid-base treatment) is a more effective approach for the synthesis of mesoporous zeolites and even other advanced materials. As a result, ABB type zeolites and their preparation method can be expanded into more fields, such as adsorbents, catalysts, and ceramics. In the following studies, we will further optimize the preparation procedure and elucidate the mechanism of adsorption process.

## CRediT authorship contribution statement

**Xuefeng Li** conducted the main experiments and wrote the total manuscript. **Shanshan Li** made a part of experiments. Both authors reviewed the manuscript.

## Declaration of competing interest

The authors declare that they have no known competing financial interests or personal relationships that could have appeared to influence the work reported in this paper.

## Declaration of Generative AI and AI-assisted technologies in the writing process

The authors confirm that there was no use of artificial intelligence (AI)-assisted technology for assisting in the writing or editing of the manuscript and no images were manipulated using AI.

## Acknowledgment

Overseas Students Science and Technology Activities Project Merit Funding in Henan Province (202115)

## References

1. Pam, A.A., Hir, Z.A.M., Abdullah, A.H., Tan, Y.P., 2021. Pb(II) removal in water via adsorption onto deep eutectic solvent fabricated activated carbon. *Applied Water Science*, **11**, 90. https://doi.org/10.1007/s13201-021-01420-6
2. Nnaji, N.D., Onyeaka, H., Miri, T., Ugwa, C., 2023. Bioaccumulation for heavy metal removal: a review. *SN Applied Sciences*, **5**. https://doi.org/10.1007/s42452-023-05351-6
3. Iqbal, A., Bonasi, K.S., 2024. A critical review on the removal of lead (heavy metal) by using various adsorbents from aqueous solution. *Environmental science and pollution research international*, 2024 Nov 14. https://doi.org/10.1007/s11356-024-35491-0
4. Bakhtiari, S., Salari, M., Shahrashoub, M., Zeidabadinejad, A., Sharma, G., Sillanpää, M., 2024. A comprehensive review on green and eco-friendly nano-adsorbents for the removal of heavy metal ions: Synthesis, adsorption mechanisms, and applications. *Current Pollution Reports*, **10**, 1-39. https://doi.org/10.1007/s40726-023-00290-7
5. Praipipat, P., Ngamsurach, P., Pratumkaew, K., 2023. The synthesis, characterizations, and lead adsorption studies of chicken eggshell powder and chicken eggshell powder-doped iron (III) oxide-hydroxide. *Arabian Journal of Chemistry*, **16**, 104640. https://doi.org/10.1016/j.arabjc.2023.104640
6. Wang, H., Wang, X., Ma, J., Xia, P., Zhao, J., 2017. Removal of cadmium (II) from aqueous solution: A comparative study of raw attapulgite clay and a reusable waste–struvite/attapulgite obtained from nutrient-rich wastewater. *Journal of Hazardous Materials*, **329**, 66-76. https://doi.org/10.1016/j.jhazmat.2017.01.025
7. Kaykhaii, M., Hashemi, S.H., Andarz, F., Piri1, A., Sargazi G., 2021. Chromium-based metal organic framework for pipette tip micro-solid phase extraction: an efective approach for determination of methyl and propyl parabens in wastewater and shampoo samples. *BMC Chemistry* **15**, 60. https://doi.org/10.1186/s13065-021-00786-7
8. Kaykhaii, M., Yavari, E., Sargazi, G., Ebrahimi, A.K., 2020. Highly sensitive determination of Bisphenol A in bottled water samples by HPLC after its extraction by a novel Th-MOF pipette-tip micro-SPE. *Journal of Chromatographic Science*, **58**, 373-382. https://doi.org/10.1093/chromsci/bmz111
9. Shahryari, T., Vahidipour, F., Chauhan, N.P.S., Sargazi, G., 2020. Synthesis of a novel Zn-MOF/PVA nanofibrous composite as bioorganic material: Design, systematic study and an efficient arsenic removal. *Polymer Engineering & Science*, **60**, 2793-2803. https://doi.org/10.1002/pen.25510
10. Khan, S., Idrees, M., Bilal, M., 2021. Revealing and elucidating chemical speciation mechanisms for lead and nickel adsorption on zeolite in aqueous solutions. *Colloids and Surfaces A: Physicochemical and Engineering Aspects*, **623**, 126711. https://doi.org/10.1016/j.colsurfa.2021.126711
11. Sellaoui, L., Hessou, E.P., Badawi, M., Netto, M.S., Dotto, G.L., Silva, L.F.O., Tielens, F., Ifthikar, J., Bonilla-Petriciolet, A., Chen, Z., 2021. Trapping of $Ag^{+}$, $Cu^{2+}$, and $Co^{2+}$ by faujasite zeolite Y: New interpretations of the adsorption mechanism via DFT and statistical modeling investigation. *Chemical Engineering Journal*, **420**, 127712. https://doi.org/10.1016/j.cej.2020.127712
12. Nguyen, N.A., Nguyen, D.K., Dinh, V.P., Duong, B.N., Ton-That, L., Hung, N.T., Ho, T.H., 2023. Effective adsorption of Pb (II) ion from aqueous solution onto ZSM-5 zeolite synthesized from Vietnamese bentonite clay. *Environmental monitoring and assessment*, **195**, 1530. https://doi.org/10.1007/s10661-023-12153-1
13. Ishihara, A., Ninomiya, M., Hashimoto, T., Nasu, H., 2020. Catalytic cracking of $C_{12}$-$C_{32}$ hydrocarbons by hierarchical β- and Y-zeolite-containing mesoporous silica and silica-alumina using Curie point pyrolyzer. *Journal of Analytical and Applied Pyrolysis*, **150**, 104876. https://doi.org/10.1016/j.jaap.2020.104876
14. Li, S., Yang, H., Wang, S., Dong, M., Wang, J., Fan, W., 2022. Facile synthesis of hierarchical macro/microporous ZSM-5 zeolite with high catalytic stability in

methanol to olefins. *Microporous and Mesoporous Materials*, **329**, 111538. https://doi.org/10.1016/j.micromeso.2021.111538
15. Rasamimanana, S., Mignard, S., Batonneau-Gener, I., 2016. Hierarchical zeolites as adsorbents for mesosulfuron-methyl removal in aqueous phase. *Microporous and Mesoporous Materials*, **226**, 153-161. https://doi.org/10.1016/j.micromeso.2015.12.014
16. Popaliya, M., Mishra, A., 2023. Modified zeolite as an adsorbent for dyes, drugs, and heavy metal removal: a review. *International Journal of Environmental Science and Technology*, **20**, 12919-12936. https://doi.org/10.1007/s13762-022-04603-z
17. Bensafi, B.éne, Chouat, N., Maziz, A., Djafri, F., 2024. Synthesis and post-synthesis modification of Zeolite Y for improved methanol adsorption and coke formation resistance. *Silicon*, **16**, 5549-5561. https://doi.org/10.1007/s12633-024-03089-3
18. Silva, D.P.S., Santos, A.T., Ribeiro, T.R.S., Solano, J.R.S., Cavalcanti, R.K.B.C., Silva, B.J.B., Quintela, P.H.L., Silva, A.O.S., 2021. Monosodium glutamate-mediated hierarchical porous formation in LTA zeolite to enhance $CO_2$ adsorption performance. *Journal of Sol-Gel Science and Technology*, **100**, 360-372. https://doi.org/10.1007/s10971-021-05644-5
19. Aghel, B., Mohadesi, M., Gouran, A., Razmegir, M.H., 2020. Use of modified iranian clinoptilolite zeolite for cadmium and lead removal from oil refinery wastewater. *International Journal of Environmental Science and Technology*, **17**, 1239-1250. https://doi.org/10.1007/s13762-019-02466-5
20. Sulaiman, K.O., Sajid, M., Alhooshani, K., 2020. Application of porous membrane bag enclosed alkaline treated Y-zeolite for removal of heavy metal ions from water. *Microchemical Journal*, **152**, 104289. https://doi.org/10.1016/j.microc.2019.104289
21. Zhang, L., Ren, Z., Dong, X., Zhao, Y., Cen, Q., 2023. Fabrication of hierarchically porous CHA-type zeolite composites derived from industrial solid waste for cesium removal. *Journal of Sol-Gel Science and Technology*, **106**, 602-615. https://doi.org/10.1007/s10971-023-06038-5
22. Jin, Y., Xiao, C., Liu, J., Zhang, S., Asaoka, S., Zhao, S., 2015. Mesopore modification of beta zeolites by sequential alkali and acid treatments: Narrowing mesopore size distribution featuring unimodality and mesoporous texture properties estimated upon a mesoporous volumetric model. *Microporous and Mesoporous Materials*, **218**, 180-191. https://doi.org/10.1016/j.micromeso.2015.07.021
23. Yu, L., Huang, S., Miao, S., Chen, F., Zhang, S., Liu, Z., Xie, S., Xu, L., 2015. A facile top-down protocol for postsynthesis modification of hierarchical aluminum-rich MFI zeolites. *Chemistry (Weinheim an der Bergstrasse, Germany)*, **21**, 1048-1054. https://doi.org/10.1002/chem.201404817
24. Jin, Y., Zhang, L., Liu, J., Zhang, S., Sun, S., Asaoka, S., Fujimoto, K., 2017. Mesopore modification of beta zeolites by sequential alkali and acid treatments: Composition-dependent T-atoms removal behavior back donating to hierarchical structure and catalytic activity in benzene alkylation. *Microporous and Mesoporous Materials*, **248**, 7-17. https://doi.org/10.1016/j.micromeso.2017.04.013
25. Huang, Y., Wang, M., Huang, Y., Shang, J., Liu, B., 2023. Mesoporous Beta zeolites with controlled distribution of Brønsted acid sites for alkylation of benzene with cyclohexene. *Results in Engineering*, **19**, 101377. https://doi.org/10.1016/j.rineng.2023.101377
26. Luo, Y., Li, M., Lv, X., Huang, Q., Chen, X., 2020. Fast synthesis of hierarchical nanosized pure Si-Beta zeolite via a steam-assisted conversion method. *Microporous and Mesoporous Materials*, **293**, 109675. https://doi.org/10.1016/j.micromeso.2019.109675
27. Sing, K., Everett, D., Haul, R., Moscou, L., Pierotti, R., Rouquerol, J., Siemieniewska, T., 1985. Reporting physisorption data for gas/solid systems with special reference to the determination of surface area and porosity. *Pure and Applied Chemistry*, **57**, 603–619. http://dx.doi.org/10.1351/pac198557040603
28. Fernandez, S., Ostraat, M.L., Lawrence, J.A., Zhang, K., 2018. Tailoring the hierarchical architecture of beta zeolites using base leaching and pore-directing agents. *Microporous and Mesoporous Materials*, **263**, 201-9. https://doi.org/10.1016/j.micromeso.2017.12.023
29. Li, X.-D., Zhai, Q.-Z., 2020. Use of nanometer mesoporous MCM-41 for the removal of Pb (II) from aqueous solution. *Applied Water Science*, **10**, 122. https://doi.org/10.1007/s13201-020-01203-5
30. He, P., Zhang, Y., Zhang, X., Chen, H., 2021. Diverse zeolites derived from a circulating fluidized bed fly ash based geopolymer for the adsorption of lead ions from wastewater. *Journal of Cleaner Production*, **312**, 127769. https://doi.org/10.1016/j.jclepro.2021.127769
31. Ciesielczyk, F., Bartczak, P.ław, Jesionowski, T., 2016. Removal of cadmium(II) and lead(II) ions from model aqueous solutions using sol–gel-derived inorganic oxide adsorbent. *Adsorption*, **22**, 445-458. https://doi.org/10.1007/s10450-015-9703-7
32. Jaihan, W., Mohdee, V., Sanongraj, S., Pancharoen, U., Nootong, K., 2022. Biosorption of lead (II) from aqueous solution using Cellulose-based Bio-adsorbents prepared from unripe papaya (Carica papaya) peel waste: Removal efficiency, thermodynamics, kinetics and isotherm analysis. *Arabian Journal of Chemistry*, **15**, 103883. https://doi.org/10.1016/j.arabjc.2022.103883
33. Kua, T.L., Kooh, M.R.R., Dahri, M.K., Zaidi, N.A.H.M., Lu, Y.C.hen, Lim, L.B.L., 2020. Aquatic plant, Ipomoea aquatica, as a potential low-cost adsorbent for the effective removal of toxic methyl violet 2B dye. *Applied Water Science*, **10**, 243. https://doi.org/10.1007/s13201-020-01326-9
34. Alghamdi, A.A., Al-Odayni, A.B., Saeed, W.S., Al-Kahtani, A., Alharthi, F.A., Aouak, T., 2019. Efficient adsorption of lead (II) from aqueous phase solutions using polypyrrole-based activated carbon. *Materials (Basel, Switzerland)*, **12**, 2020. https://doi.org/10.3390/ma12122020
35. Zhang, X., Wang, B., Chang, J., 2025. Effect of $Na^+$ and $Ca^{2+}$ treatment concentrations on natural zeolite for lead adsorption behavior and solidification mechanism in highly alkaline environments. *Chemical Engineering Journal*, **503**, 158434. https://doi.org/10.1016/j.cej.2024.158434
36. Rondón, W., Freire, D., Benzo, Z.de, Sifontes, A.B., González, Y., Valero, M., Brito, J.L., 2013. Application of 3A zeolite prepared from venezuelan kaolin for removal of Pb (II) from wastewater and its determination by flame atomic absorption spectrometry. *American Journal of Analytical Chemistry*, **04**, 584-593. https://doi.org/10.4236/ajac.2013.410069
37. Rakhym, A.B., Seilkhanova, G..A., Kurmanbayeva, T.S., 2020. Adsorption of lead (II) ions from water solutions with natural zeolite and chamotte clay. *Materials Today: Proceedings*, **31**, 482-5. https://doi.org/10.1016/j.matpr.2020.05.672
38. Mahmood, U., Alkorbi, A.S., Hussain, T., Nazir, A., Qadir, M.B., Khaliq, Z., Faheem, S., Jalalah, M., 2024. Adsorption of lead ions from wastewater using electrospun zeolite/MWCNT nanofibers: Kinetics, thermodynamics and modeling study. *RSC Advances*, **14**, 5959-5974. https://doi.org/10.1039/d3ra07720a
39. Shilawati Ehishan, N., Sapawe, N., 2018. Performance studies removal of chromium ($Cr^{6+}$) and lead ($Pb^{2+}$) by oil palm frond (OPF) adsorbent in aqueous solution. *Materials Today: Proceedings*, **5**, 21897-21904. https://doi.org/10.1016/j.matpr.2018.07.048
40. Yasmeen, K., Nawaz, S., Iqbal, A., Siddiqui, A., Umar, A.R., Muhammad, H., Shafique, M., Shah, F., Tahir, S., Khan, A.M., Masab, M., Hanif, M., 2022. Removal of Pb (II) from water samples using surface modified core/shell CdZnS/ZnS QDs as adsorbents: Characterization, adsorption, kinetic and thermodynamic studies. *Arabian Journal of Chemistry*, **15**, 104224. https://doi.org/10.1016/j.arabjc.2022.104224